Journal of Sound and Vibration (2003) **259**(4), 761–777
doi:10.1006/jsvi.2002.5113, available online at http://www.idealibrary.com on IDEAL®

ON THE ACOUSTIC ABSORPTION OF MULTI-LAYER ABSORBERS WITH DIFFERENT INNER STRUCTURES

F.-C. Lee and W.-H. Chen

Department of Power Mechanical Engineering, National Tsing Hua University, Hsinchu, Taiwan 30043*, Republic of China. E-mail: whchen@pme.nthu.edu.tw*

(*Received* 18 *June* 2001, *and in final form* 10 *April* 2002)

A rigorous finite element analysis procedure is developed to study the effect of the inner structures on the acoustic absorption of multi-layer absorbers. To do this, four types of basic inner structure compartments adopted in the multi-layer absorbers are selected for analysis. These compartments are composed of porous materials inlaid with perforated plates of various shapes, say, triangle, semicircle, convex rectangle and plate shapes. As it is different from the conventional finite element analysis for the acoustic system in the literature, the perforated plates are simulated by appropriate equivalent boundary conditions, depending on their thickness, hole radius, hole pitch and porosity and the air contained in the holes. A large number of total degrees of freedom generated from meshing the air in the holes of perforated plates are thus avoided. The results reveal that the inner structures of the multi-layer absorbers will influence the acoustic absorption at some frequency bands significantly. Based on those features, the multi-layer absorber with a novel inner structure is then designed and manufactured. Both the finite element and experimental results show that its acoustic absorption would be distinctly promoted.

1. INTRODUCTION

In recent years, the use of multi-layer absorbers has become increasingly important in noise abatement. In general, to ensure the acoustic absorption of the multi-layer absorbers, selecting appropriate absorbing materials [1–4] is the primary concern. Several recent literatures [5–7] depicted that the surface shapes of absorbing materials also control the performance of the acoustic absorption. However, there are still seldom investigations on the influence of the inner structures employed in the multi-layer absorbers. One of the main objectives of this work is thus to study the effect of the inner structures on the acoustic absorption of the multi-layer absorbers.

In early works, Ross [8, 9] provided a finite element model to analyze the transmission loss of automotive mufflers composed of expansion chamber and perforated tubes. The perforated tubes were simulated as many perforated plates in the finite element model and an equivalent boundary was devised to represent the acoustic effect of the perforated plates. Although both the air and perforated plates were tackled in this finite element model, the porous materials were not included. Easwaran and Munjal [5] presented another finite element model to analyze the acoustic absorption of the wedge absorber used in an anechoic chamber. The materials and air were involved in such acoustic system, yet the perforated plates were not accounted for. Recently, the authors [7] established a finite element procedure to deal with the acoustic absorbers that simultaneously contained perforated plates, porous materials and air. However, a large number of total degrees of

0022-460X/02/$35.00

freedom were generated from meshing the air in the holes of the perforated plates. Therefore, to study the effect of the inner structures on the acoustic absorption of the multi-layer absorbers, a modified finite element model that can effectively deal with the combined effects of perforated plates, porous materials and air is imperative.

In the present work, the merits of Ross's [8, 9] or Easwaran and Munjal's [5] finite element models are also adopted. For example, as compared with the conventional finite element model [7] in the analysis of multi-layer absorbers, the present finite element model is more effective since the equivalent perforated plate boundary is employed. In addition, the acoustic effect on the equivalent perforated plate boundary is described by its acoustic impedance [10], depending on the thickness, hole radius, hole pitch and porosity of the perforated plate and the air contained in the holes. As for modelling the porous materials in the present finite element model, their acoustic properties are represented by the complex wave propagation constant and characteristic impedance in terms of flow resistivity, wave number, air density and sound frequency [2]. Therefore, the multi-layer absorbers studied can be well simulated and analyzed.

Four types of basic inner structure compartments used in the multi-layer absorbers are analyzed to demonstrate their geometrical effects on the acoustic absorption. As shown in Figure 1, these compartments are composed of porous materials inlaid with perforated plates of various shapes, say, triangle, semicircle, convex rectangle and plate shapes. Some typical multi-layer absorbers can be thus assembled from these compartments (see Figure 2). The computed normal-incident acoustic absorption coefficients of these assemblies depict that different inner structures of the multi-layer absorbers will affect the acoustic absorption at some frequency bands distinctly. With the motivation of these results, a novel design of the inner structure for the multi-layer absorbers is also proposed.

To verify the simulated results, relevant experiments are also performed. The two-microphone impedance tube system [7] is applied to measure the acoustic absorption coefficients of the multi-layer absorbers manufactured.

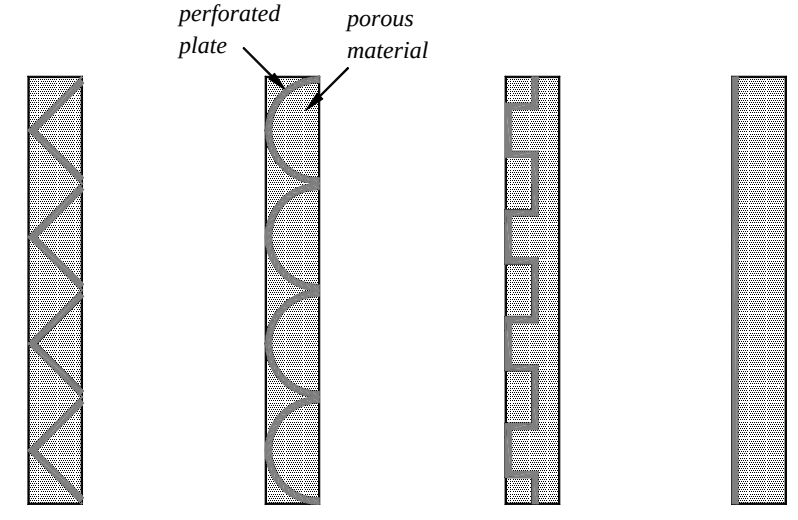

Figure 1. Various basic inner structure compartments.

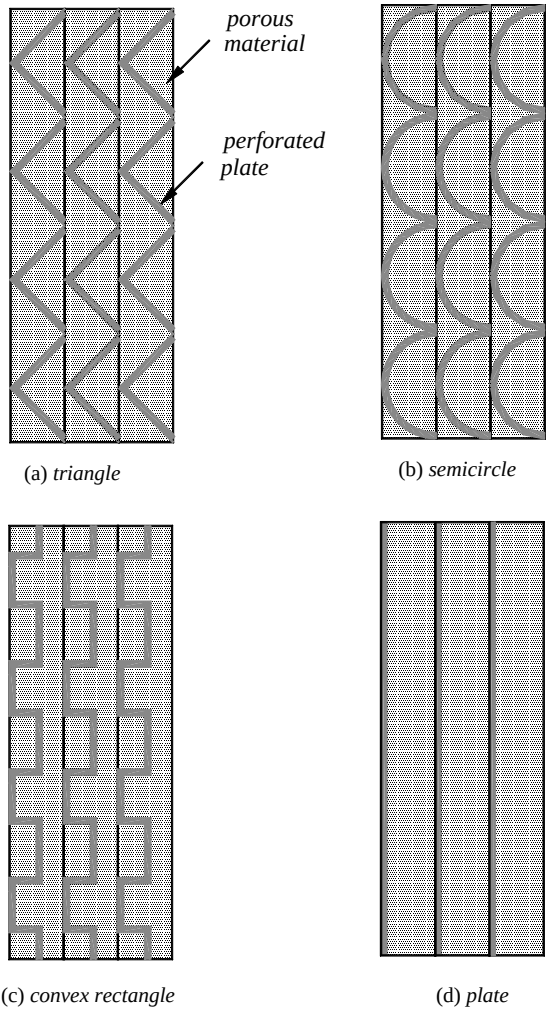

Figure 2. The multi-layer absorbers with various types of compartments.

2. THEORY

2.1. GOVERNING EQUATIONS OF SOUND PROPAGATION

In this work, the porous materials are treated as an equivalent fluid. Hence, some important parameters, such as the complex wave propagation constant and complex density, are represented in complex form. These parameters are analogous to those (the wave propagation constant and density) in air. Therefore, the sound propagations in the air and porous materials are both governed by the Helmholtz wave propagation equation as [5]

$$\nabla^2 P_j + k_j^2 P_j = 0 \quad \text{in } \Omega_j \ \ (j = a \text{ or } m), \tag{1}$$

where (Ω_a, Ω_m), (P_a, P_m) and (k_a, k_m) are, respectively, the domains, sound pressures and wave numbers of the air and porous materials. $k_a = \omega/c_a$ and $k_m = -\mathrm{i}\gamma$, where c_a is the sound speed in air, ω is the angular frequency of excitation and γ is the complex wave propagation constant.

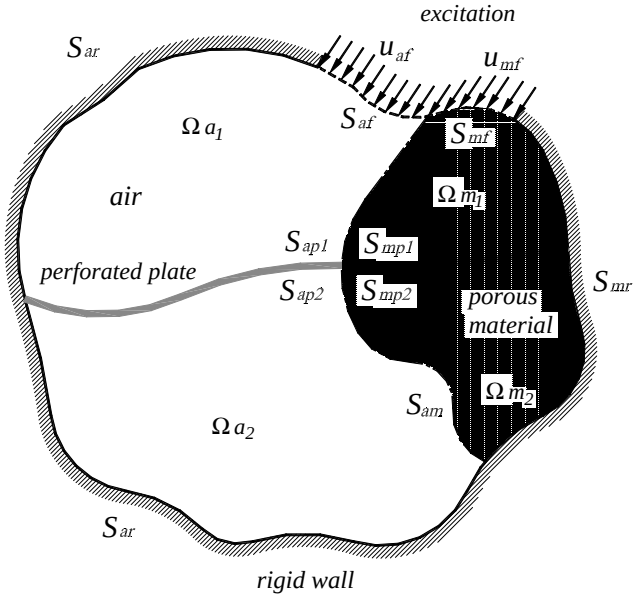

Figure 3. A general configuration of the acoustic system.

2.2. BOUNDARY CONDITIONS

A general configuration of the considered model is shown in Figure 3. The boundary conditions can be quoted as follows:

(a) For the rigid wall boundary S_{jr} ($j = a$ or m),

$$\frac{\partial P_j}{\partial n} = 0 \quad \text{on } S_{jr} \ (j = a \text{ or } m). \tag{2}$$

(b) For the interface S_{am} between air and porous materials,

$$\vec{n}_a \cdot \vec{u}_a = -\vec{n}_m \cdot \vec{u}_m \tag{3}$$

and

$$\frac{\partial P_j}{\partial n} = -\mathrm{i}\rho_j \omega \, \vec{u}_j \cdot \vec{n}_j \quad \text{on } S_{am} \ (j = a \text{ or } m), \tag{4}$$

where $\vec{n}_a$ and $\vec{n}_m$ are, respectively, the outward unit vectors normal to the interface S_{am}. $\vec{u}_a$ and $\vec{u}_m$ are the particle velocity vectors of air and porous materials at the interface S_{am} respectively. ρ_a is the density of air and ρ_m is the complex density of porous materials [5].

(c) For the external excitation boundary S_{jf} ($j = a$ or m),

$$\frac{\partial P_j}{\partial n} = -i\rho_j \omega u_{jf} \quad \text{on } S_{jf} \ (j = a \text{ or } m), \tag{5}$$

where u_{af} and u_{mf} are, respectively, the external excitation particle velocity on the boundary S_{af} and S_{mf}.

(d) For the equivalent perforated plate boundary S_{jp1} and S_{jp2} ($j = a$ or m) [8,9],

$$\frac{\partial P_{j1}}{\partial n} = -\mathrm{i}\frac{k_j}{Z_p}(P_{j1} - P_{j2}) \quad \text{on } S_{jp1} \ (j = a \text{ or } m) \tag{6}$$

and

$$\frac{\partial P_{j2}}{\partial n} = -\mathrm{i}\frac{k_j}{Z_p}(P_{j2} - P_{j1}) \quad \text{on } S_{jp2} \ (j = a \text{ or } m), \tag{7}$$

where P_{j1} and P_{j2} ($j = a$ or m) are, respectively, the sound pressures on the perforated plate boundary S_{jp1} and S_{jp2} ($j = a$ or m). Z_p is the acoustic impedance of the perforated plate and is given as [10]

$$Z_p = \frac{\rho_a}{\varepsilon}\sqrt{8\nu\omega}\left(1 + \frac{t_p}{2a}\right) + \mathrm{i}\frac{\omega\rho_a}{\varepsilon}\left[\sqrt{\frac{8\nu}{\omega}}\left(1 + \frac{t_p}{2a}\right) + t_p + \delta\right], \tag{8}$$

where ν is the kinematic viscosity of air ($\nu = 15 \times 10^{-6}\,\mathrm{m^2/s}$ at room temperature). t_p, a, ε ($= \pi a^2/b^2$) and δ ($= 1{\cdot}7a\phi(\varepsilon)$) are the thickness, hole radius, porosity and viscous boundary layer thickness of the perforated plate respectively. b is the hole pitch of the perforated plate and $\phi(\varepsilon) = 1 - 1{\cdot}47\sqrt{\varepsilon} + 0{\cdot}47\sqrt{\varepsilon^3}$.

2.3. GALERKIN FINITE ELEMENT FORMULATION

The present finite element model is derived based on the Galerkin analysis method. Similar to the Galerkin finite element analysis procedure used by Easwaran and Munjal [5], a set of shape functions chosen in the domain and on the boundary have been taken as the weighting functions for the governing equation and boundary conditions. Combining the weighted residual statement in the domain Ω_j ($j = a$ or m), one can obtain

$$\begin{aligned}
&\int_{\Omega_j} N_j(\nabla^2 P_j + k_j^2 P_j)\,\mathrm{d}\Omega_j + \int_{S_{jr}} \bar{N}_j\left(\frac{\partial P_j}{\partial n}\right)\mathrm{d}S_j \\
&+ \int_{S_{am}} \bar{N}_j\left(\frac{\partial P_j}{\partial n} + \mathrm{i}\rho_j\omega\,\vec{n}_j{\cdot}\vec{u}_j\right)\mathrm{d}S_j + \int_{S_{jp1}} \bar{N}_j\left(\frac{\partial P_{j1}}{\partial n} + \mathrm{i}\frac{k_j}{Z_p}(P_{j1} - P_{j2})\right)\mathrm{d}S_j \\
&+ \int_{S_{jp2}} \bar{N}_j\left(\frac{\partial P_{j2}}{\partial n} + \mathrm{i}\frac{k_j}{Z_p}(P_{j2} - P_{j1})\right)\mathrm{d}S_j + \int_{S_{jf}} \bar{N}_j\left(\frac{\partial P_j}{\partial n} + \mathrm{i}\rho_j\omega u_{jf}\right)\mathrm{d}S_j = 0,
\end{aligned} \tag{9}$$

where N_j and $\overline{N_j}$ ($j = a$ or m) are the shape functions in the domain and on the boundary respectively. Using the first form of Green's theorem, the first term in equation (9) can be written as

$$\begin{aligned}
\int_{\Omega_j} N_j\nabla^2 P_j\,\mathrm{d}\Omega_j &= \int_{\Omega_j} \nabla{\cdot}(\nabla P_j N_j)\,\mathrm{d}\Omega_j - \int_{\Omega_j} \nabla P_j{\cdot}\nabla N_j\,\mathrm{d}\Omega_j \\
&= \int_{S_{jt}} N_j\frac{\partial P_j}{\partial n}\,\mathrm{d}S_j - \int_{\Omega_j} \nabla P_j{\cdot}\nabla N_j\,\mathrm{d}\Omega_j.
\end{aligned} \tag{10}$$

Substituting the above equation into equation (9) yields

$$\begin{aligned}
&\left[-\int_{\Omega_j} (\nabla N_j{\cdot}\nabla P_j - k_j^2 N_j P_j)\,\mathrm{d}\Omega_j + \int_{S_{jt}} N_j\left(\frac{\partial P_j}{\partial n}\right)\mathrm{d}S_j\right] + \int_{S_{jr}} \bar{N}_j\left(\frac{\partial P_j}{\partial n}\right)\mathrm{d}S_j \\
&+ \int_{S_{am}} \bar{N}_j\left(\frac{\partial P_j}{\partial n} + \mathrm{i}\rho_j\omega\,\vec{n}_j{\cdot}\vec{u}_j\right)\mathrm{d}S_j + \int_{S_{jp1}} \bar{N}_j\left(\frac{\partial P_{j1}}{\partial n} + \mathrm{i}\frac{k_j}{Z_p}(P_{j1} - P_{j2})\right)\mathrm{d}S_j \\
&+ \int_{S_{jp2}} \bar{N}_j\left(\frac{\partial P_{j2}}{\partial n} + \mathrm{i}\frac{k_j}{Z_p}(P_{j2} - P_{j1})\right)\mathrm{d}S_j + \int_{S_{jf}} \bar{N}_j\left(\frac{\partial P_j}{\partial n} + \mathrm{i}\rho_j\omega u_{jf}\right)\mathrm{d}S_j = 0,
\end{aligned} \tag{11}$$

where S_{jt} ($j = a$ or m) is the total boundary involving S_{am}, S_{jr}, S_{jf}, S_{jp1} and S_{jp2} ($j = a$ or m). Choosing the shape functions on the boundary such that $\bar{N}_j = -N_j$ ($j = a$ or m) yields

$$\int_{\Omega_j} (\nabla N_j \cdot \nabla P_j - k_j^2 N_j P_j)\, \mathrm{d}\Omega_j + \int_{S_{am}} N_j (\mathrm{i}\rho_j \omega \vec{n}_j \cdot \vec{u}_j)\, \mathrm{d}S_j + \int_{S_{jp1}} N_j \left(\mathrm{i}\frac{k_j}{Z_p}(P_{j1} - P_{j2}) \right) \mathrm{d}S_j + \int_{S_{jp2}} N_j \left(\mathrm{i}\frac{k_j}{Z_p}(P_{j2} - P_{j1}) \right) \mathrm{d}S_j + \int_{S_{jf}} N_j (\mathrm{i}\rho_j \omega u_{jf})\, \mathrm{d}S_j = 0. \tag{12}$$

Let equation (12) for the porous material be multiplied by ρ_a/ρ_m and be added with equation (12) for air. Using the boundary condition $\vec{n}_a \cdot \vec{u}_a = -\vec{n}_m \cdot \vec{u}_m$ yields

$$\int_{\Omega_a} (\nabla N_a \cdot \nabla P_a - k_a^2 N_a P_a)\, \mathrm{d}\Omega_a + \frac{\rho_a}{\rho_m} \int_{\Omega_m} (\nabla N_m \cdot \nabla P_m - k_m^2 N_m P_m)\, \mathrm{d}\Omega_m + \int_{S_{ap1}} N_a \left(\mathrm{i}\frac{k_a}{Z_p}(P_{a1} - P_{a2}) \right) \mathrm{d}S_a + \int_{S_{ap2}} N_a \left(\mathrm{i}\frac{k_a}{Z_p}(P_{a2} - P_{a1}) \right) \mathrm{d}S_a + \frac{\rho_a}{\rho_m} \int_{S_{mp1}} N_m \left(\mathrm{i}\frac{k_m}{Z_p}(P_{m1} - P_{m2}) \right) \mathrm{d}S_m + \frac{\rho_a}{\rho_m} \int_{S_{mp2}} N_m \left(\mathrm{i}\frac{k_m}{Z_p}(P_{m2} - P_{m1}) \right) \mathrm{d}S_m = -\mathrm{i}\rho_a \omega \left(\int_{S_{af}} N_a u_{af}\, \mathrm{d}S_a + \int_{S_{mf}} N_m u_{mf}\, \mathrm{d}S_m \right). \tag{13}$$

Let the sound pressures be expressed in terms of the nodal sound pressures and shape functions. Equation (13) is written in matrix forms as

$$\sum_{e=1}^{n_a} \int_{\Omega_{ae}} (\nabla \{N\}_a \cdot \nabla \{N\}_a^{\mathrm{T}} \{P\}_a - k_a^2 \{N\}_a \{N\}_a^{\mathrm{T}} \{P\}_a)\, \mathrm{d}\Omega_{ae} + \sum_{e=1}^{n_m} \frac{\rho_a}{\rho_m} \int_{\Omega_{me}} (\nabla \{N\}_m \cdot \nabla \{N\}_m^{\mathrm{T}} \{P\}_m - k_m^2 \{N\}_m \{N\}_m^{\mathrm{T}} \{P\}_m)\, \mathrm{d}\Omega_{me} + \sum_{e=1}^{n_{ap1}} \mathrm{i}\frac{k_a}{Z_p} \left(\int_{S_{ap1e}} \{N\}_a \{N\}_a^{\mathrm{T}} \{P\}_{ap1}\, \mathrm{d}S_{ae} - \int_{S_{ap2e}} \{N\}_a \{N\}_a^{\mathrm{T}} \{P\}_{ap1}\, \mathrm{d}S_{ae} \right) + \sum_{e=1}^{n_{ap2}} \mathrm{i}\frac{k_a}{Z_p} \left(\int_{S_{ap2e}} \{N\}_a \{N\}_a^{\mathrm{T}} \{P\}_{ap2}\, \mathrm{d}S_{ae} - \int_{S_{ap1e}} \{N\}_a \{N\}_a^{\mathrm{T}} \{P\}_{ap2}\, \mathrm{d}S_{ae} \right) + \sum_{e=1}^{n_{mp1}} \mathrm{i}\frac{\rho_a}{\rho_m}\frac{k_m}{Z_p} \left(\int_{S_{mp1e}} \{N\}_m \{N\}_m^{\mathrm{T}} \{P\}_{mp1}\, \mathrm{d}S_{me} - \int_{S_{mp2e}} \{N\}_m \{N\}_m^{\mathrm{T}} \{P\}_{mp1}\, \mathrm{d}S_{me} \right) + \sum_{e=1}^{n_{mp2}} \mathrm{i}\frac{\rho_a}{\rho_m}\frac{k_m}{Z_p} \left(\int_{S_{mp2e}} \{N\}_m \{N\}_m^{\mathrm{T}} \{P\}_{mp2}\, \mathrm{d}S_{me} - \int_{S_{mp1e}} \{N\}_m \{N\}_m^{\mathrm{T}} \{P\}_{mp2}\, \mathrm{d}S_{me} \right) = -\mathrm{i}\rho_a \omega \left(\sum_{e=1}^{n_{af}} \int_{S_{afe}} \{N\}_a u_{af}\, \mathrm{d}S_{ae} + \sum_{e=1}^{n_{mf}} \int_{S_{mfe}} \{N\}_m u_{mf}\, \mathrm{d}S_{me} \right), \tag{14}$$

where n_a, n_m, n_{ap1}, n_{ap2}, n_{mp1}, n_{mp2}, n_{af} and n_{mf} denote the element numbers of discretization in the domain Ω_a and Ω_m and on the boundary S_{ap1}, S_{ap2}, S_{mp1}, S_{mp2}, S_{af} and S_{mf} respectively. $\{P\}_j$ ($j = a$ or m) is the nodal sound pressure in the region $\Omega_j + S_{jr} + S_{jf}$ ($j = a$ or m). $\{P\}_{jp1}$ and $\{P\}_{jp2}$ ($j = a$ or m) are the nodal sound pressures on the equivalent perforated plate boundary S_{jp1} and S_{ap2} ($j = a$ or m). In this work, eight-node brick elements are employed. The shape functions $\{N\}_j$ ($j = a$ or m) can be readily found in literatures [8,9]

Let the nodal sound pressures $\{P\}_{jt}$ ($j = a$ or m) be the assembly of $\{P\}_j$, $\{P\}_{jp1}$ and $\{P\}_{jp2}$ ($j = a$ or m), and

$$[K]_j = \sum_{e=1}^{n_j} \int_{\Omega_{je}} (\nabla\{N\}_j \cdot \nabla\{N\}_j^{\mathrm{T}})\, \mathrm{d}\Omega_{je} \quad (j = a \text{ or } m), \tag{15}$$

$$[M]_j = \sum_{e=1}^{n_j} \int_{\Omega_{je}} (\{N\}_j \{N\}_j^{\mathrm{T}})\, \mathrm{d}\Omega_{je} \quad (j = a \text{ or } m), \tag{16}$$

$$\{F\}_j = \sum_{e=1}^{n_{jf}} -\mathrm{i}\rho_a \omega \int_{S_{jfe}} \{N\}_j u_{jf}\, \mathrm{d}S_{je} \quad (j = a \text{ or } m), \tag{17}$$

$$[C]_{j1} = \sum_{e=1}^{n_{jp1}} \int_{S_{jp1e}} \{N\}_j \{N\}_j^{\mathrm{T}}\, \mathrm{d}S_{je} \quad (j = a \text{ or } m) \tag{18}$$

and

$$[C]_{j2} = \sum_{e=1}^{n_{jp2}} \int_{S_{jp2e}} \{N\}_j \{N\}_j^{\mathrm{T}}\, \mathrm{d}S_{je} \quad (j = a \text{ or } m), \tag{19}$$

then equation (14) can be rearranged as

$$\lfloor [T]_a \quad [T]_m \quad [T]_c \rfloor \begin{Bmatrix} \{P\}_{at} \\ \{P\}_{mt} \\ \{P\}_c \end{Bmatrix} = \{F\}_a + \{F\}_m, \tag{20}$$

where

$$[T]_a = [K]_a - k_a^2 [M]_a + \mathrm{i}\frac{k_a}{Z_p}([C]_{a1} + [C]_{a2}), \tag{21}$$

$$[T]_m = \frac{\rho_a}{\rho_m}([K]_m - k_m^2 [M]_m + \mathrm{i}\frac{k_m}{Z_p}([C]_{m1} + [C]_{m2})) \tag{22}$$

and

$$[T]_c = \left([K]_a + \frac{\rho_a}{\rho_m}[K]_m\right) - \left(k_a^2 [M]_a + \frac{\rho_a}{\rho_m} k_m^2 [M]_m\right). \tag{23}$$

In the above, $\{P\}_c$ is the nodal pressure on the boundary S_{am}. As a result, the nodal sound pressure distribution of the entire multi-layer absorber can be evaluated by solving equation (20).

2.4. CALCULATION OF ACOUSTIC ABSORPTION COEFFICIENT α

Once the external excitation particle velocity is given as 1 m/s, the nodal sound pressure on the external excitation boundary S_{jf} ($j = a$ or m) is equivalent to the input impedance

Γ_i [3]. The acoustic absorption coefficient α can be calculated by [11]

$$\alpha = \frac{4R_r/\rho_a c_a}{(R_r/\rho_a c_a + 1)^2 + (X_r/\rho_a c_a)^2}, \tag{24}$$

where R_r and X_r, respectively, denote the real and imaginary parts of the input impedance Γ_i.

3. EXPERIMENTS

To validate the acoustic effect of the designed inner structure, the finite element calculation is also compared with the experimental results. Herein, the two- microphone impedance tube system [7] is applied to measure the acoustic absorption coefficient α of the multi-layer absorber manufactured.

The system includes an impedance tube, which contains two pieces of 1/2″ microphones and a speaker, and a personal computer system, which has the frequency analysis system and acoustic signal driver. By this system, the transfer function H_{21} $(= p_2/p_1)$ can be obtained. p_1 and p_2 are, respectively, the sound pressures measured by the first and second microphones. The experimental acoustic absorption coefficient α of the acoustic absorber sample can then be calculated by

$$\alpha = 1 - \left| \frac{H_{21} - e^{-ik_a(z_1 - z_2)}}{e^{ik_a(z_1 - z_2)} - H_{21}} e^{i2k_a z_1} \right|^2, \tag{25}$$

where z_1 (z_2) denotes the distance between the first (second) microphone and the acoustic absorber sample. In the system, the frequency range of analysis is 100–2000 Hz and the acoustic absorption coefficient α is calculated with an interval of 5 Hz.

4. RESULTS AND DISCUSSIONS

To validate the accuracy of the present finite element model for the analysis of the multi-layer absorbers involving the perforated plates, porous materials and air, the simple case

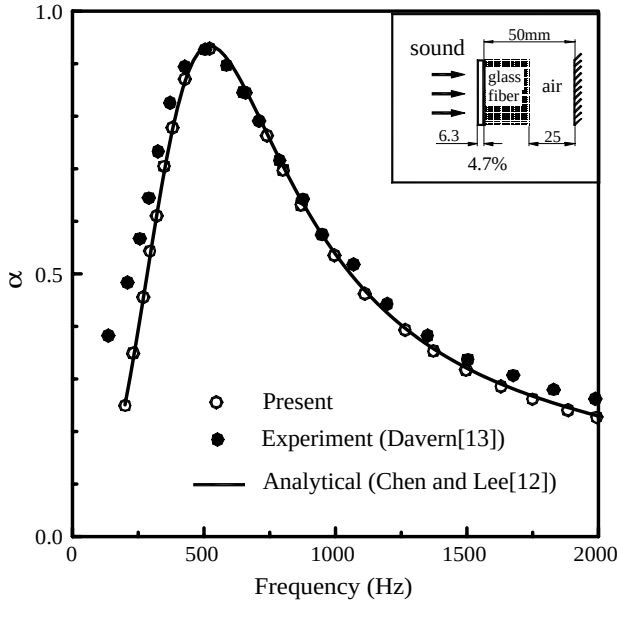

Figure 4. Comparison of the acoustic absorption coefficients by different approaches.

which has been analytically studied by the authors [12] is first analyzed and shown in Figure 4. As seen in Figure 4, the results of the present finite element model are in excellent agreement with the analytical solutions [12]. Good comparisons between the present finite element results and referenced experimental data [13] are also found.

To demonstrate the merits of the present finite element model, the case as shown in Figure 5 is then solved by the present and conventional finite element models [7] respectively. The perforated plate (thickness $t_p = 1$ mm, porosity $\varepsilon = 3{\cdot}1\%$, hole radius $a = 1$ mm and hole pitch $b = 10$ mm) is backed with the fiberglass (thickness $t_m = 50$ mm and flow resistivity $\sigma = 16\,000\ \mathrm{Ns/m^4}$). The present finite element mesh adopts eight eight-node brick elements (40 nodes) as compared with 1296 eight-node brick elements (1489 nodes) by the conventional finite element mesh. To ensure the validity and accuracy of the calculated results, the side length of elements is taken as less than 1/6 wavelength of the incident sound [14]. It is found that the numbers of elements and nodes employed in the present finite element model are both largely abated due to the equivalent perforated plate boundary devised. Figure 6 depicts that the acoustic absorption coefficients α calculated by the conventional finite element model [7] are still higher than those of the analytical

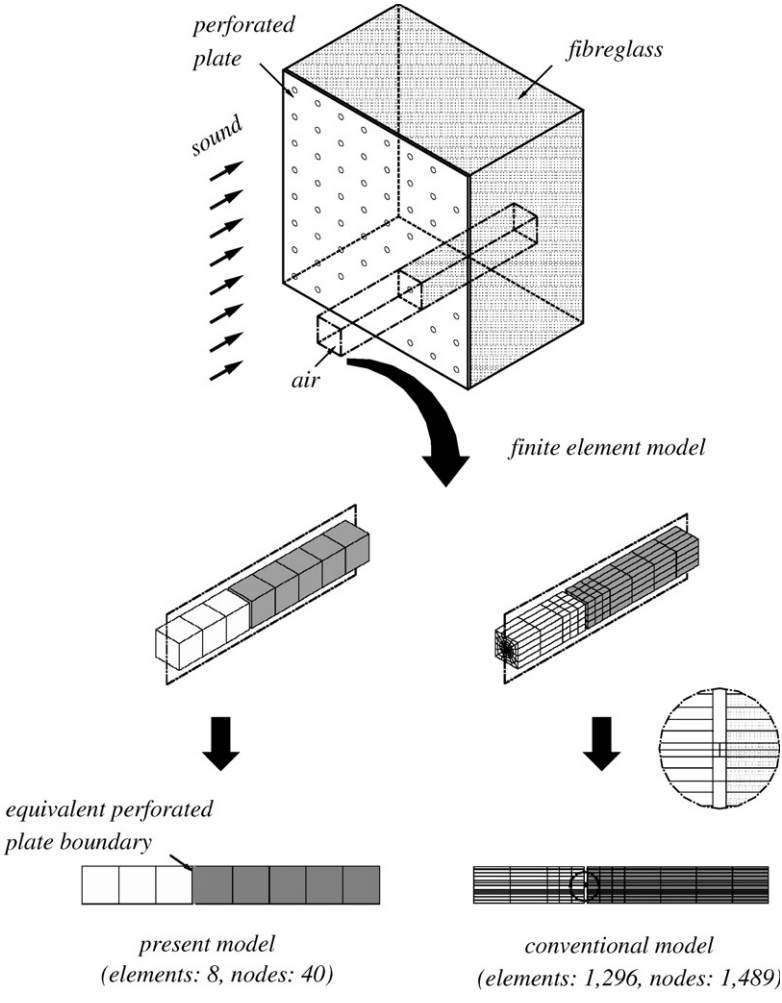

Figure 5. Comparison of the present and conventional finite element models.

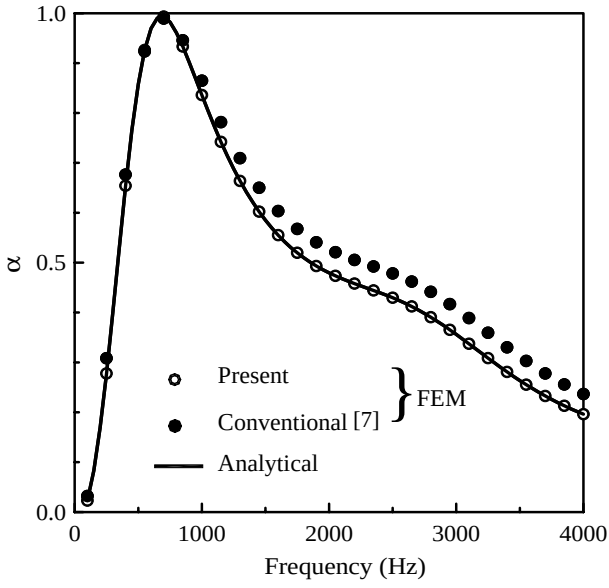

Figure 6. Comparison of the acoustic absorption coefficients by different finite element models.

solution or the present finite element model at the frequency bands over 1000 Hz. Hence, the present finite element model developed is adopted for further analyzing the multi-layer absorbers required in this work.

4.1. ACOUSTIC ABSORPTION OF VARIOUS COMPARTMENTS

To study the influence of the inner structures on the acoustic absorption, as mentioned earlier, four types of basic inner structure compartments are selected to construct the multi-layer absorbers. These basic compartments are composed of porous materials inlaid with perforated plates of various shapes, say, triangle, semicircle, convex rectangle and plate shapes. Due to symmetry, under appropriate boundary conditions as stated in section 2.2, it is sufficient to analyze a slice of each compartment [7]. The finite element meshes and dimensions of these compartments have been shown in Figure 7, where the flow resistivity of the fiberglass $\sigma = 16\,000\,\mathrm{Ns/m^4}$, the thickness of the perforated plate $t_p = 1$ mm and the porosity of perforated plate $\varepsilon = 4{\cdot}9\%$ (the hole radius $a = 0{\cdot}75$ mm and hole pitch $b = 6$ mm).

The results as displayed in Figure 8 depict that the acoustic absorption of the plate shape compartment is higher than others at the frequency bands below 1700 Hz, while the acoustic absorption of the triangle shape compartment is higher than others at frequency bands over 2200 Hz. The semicircle and convex rectangle shape compartments reveal similar acoustic absorption characteristics, except that the acoustic absorption of the convex rectangle shape compartment is slightly higher than that of the semicircle shape compartment at the frequency bands over 2200 Hz. Consequently, one can conclude that more porous materials in front of the perforated plate (for example, the triangle shape compartment) will promote the acoustic absorption at higher frequency bands. This is due to the fact that the porous material itself has advantage in absorbing incident sound at higher frequency bands [2]. In contrast, if the perforated plate backed with more porous

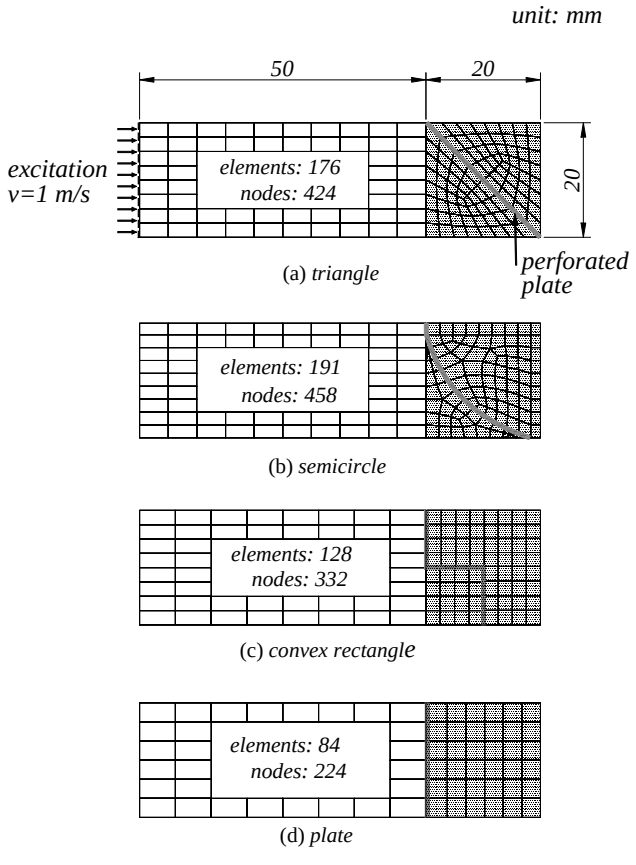

Figure 7. Finite element meshes of various compartments.

materials like the plate shape compartment, the acoustic absorption at lower frequency bands is more distinct. That is, more porous materials behind the perforated plates will induce additional acoustic resistance at lower frequency bands [13].

4.2. ACOUSTIC ABSORPTION OF VARIOUS MULTI-LAYER ABSORBERS

To further study the effect of different inner structures on the acoustic absorption of the multi-layer absorbers, as displayed in Figure 2, the multi-layer absorbers assembled with three layers of various types of compartments are also analyzed. The finite element meshes and dimensions of these multi-layer absorbers can be found in Figure 9. As shown in Figure 10, the acoustic absorption of the multi-layer absorbers composed of the triangle, semicircle or convex rectangle shape compartments would be distinctly improved at higher frequency bands (over 3000 Hz). However, the multi-layer absorber composed of the plate shape compartment still has better acoustic absorption than others at lower frequency bands (below 700 Hz). That is, as concluded in section 4.1, the quantity of the porous materials ahead of the outmost layer of perforated plates controls the acoustic absorption at high frequencies. Also, more porous materials behind the perforated plates would enhance the acoustic absorption at lower frequency bands. Owing to the total porous materials behind the outmost, middle and innermost layers of

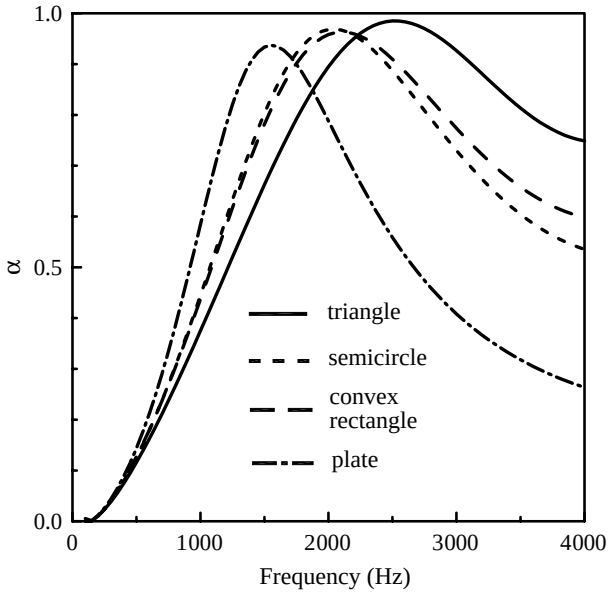

Figure 8. Comparison of the acoustic absorption coefficients for various compartments.

the perforated plate for these four multi-layer absorbers do not differ so much, the difference of the acoustic absorption of these absorbers at lower frequency bands (below 700 Hz) is not so distinct as that in Figure 8 for a single layer of basic compartment.

4.3. A NEWLY DESIGNED INNER STRUCTURE

Based on the features achieved in sections 4.1 and 4.2, a newly designed inner structure unit for the multi-layer absorber is proposed. Its dimension and outline are shown in Figure 11. Each inner structure unit, which is made of 95% hardiness PVC, contains a spiral plate and is filled with porous materials. For the effective use of the porous materials behind the spiral plate for enhancing the acoustic absorption, only a portion of the spiral plate is perforated (see Figure 11). The multi-layer absorber is thus constructed by several assembled inner structure units, surrounded by a face-perforated plate and rigid walls.

To demonstrate the acoustic absorption of the designed multi-layer absorber, without loss of the generality, a representative portion is selected for analysis. The incident sound will first pass through the face-perforated plate and then enter into the inner structure unit along the spiral plate. As motivated in sections 4.1 and 4.2, more porous materials behind the face-perforated plate will enhance the acoustic absorption at lower frequency bands, especially the spiral transmission path is much longer than the thickness of the absorber. Hence, most of the incident sound at lower frequency bands will be absorbed here. Part of the incident sound will continue to transmit the inside perforated plate. The inside perforated plate with lower porosity $\varepsilon_2 = 8{\cdot}7\%$ and the porous materials of the innermost part behind the inside perforated plate are again designed to absorb the rest of incident sound at lower frequency bands. Besides, the face-perforated plate with high porosity ($\varepsilon_1 = 19{\cdot}6\%$) is good for the acoustic absorption at higher frequency bands. Certainly, the large quantity of porous materials in front of the inside perforated plate also has the

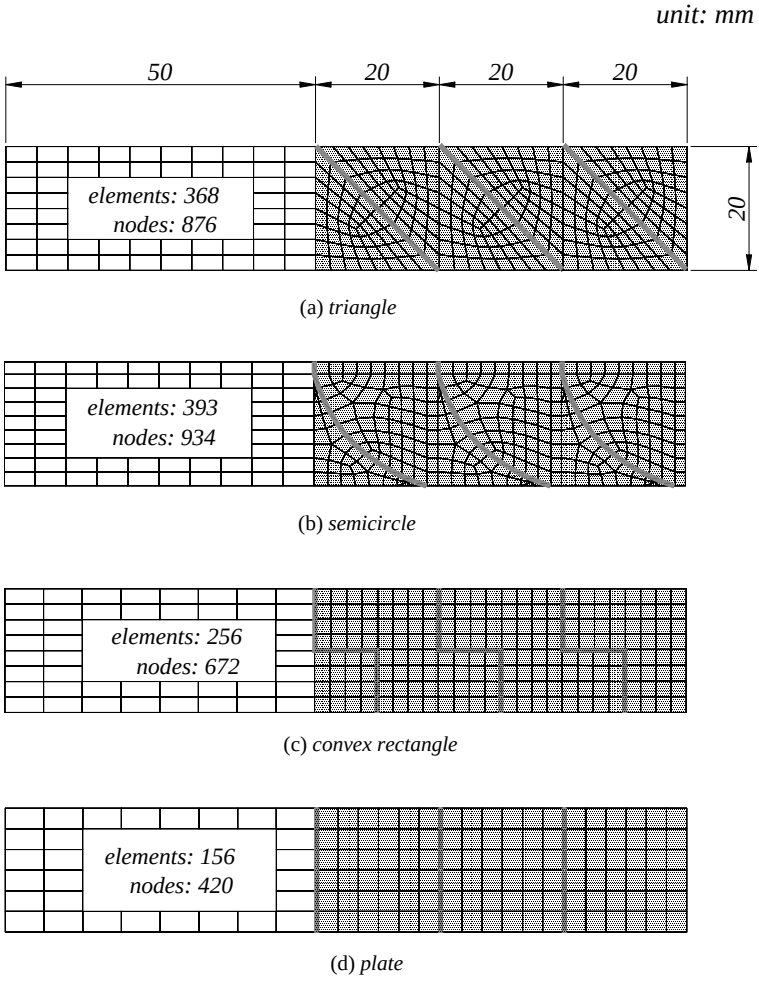

Figure 9. Finite element meshes of various multi-layer absorbers.

advantage for better acoustic absorption at higher frequency bands. Therefore, the designed multi-layer absorber can be expected to have much better acoustic absorption than conventional ones.

To examine the effects of this multi-layer absorber on the acoustic absorption, both the finite element analysis and experimental measurement are performed. Figure 11 shows the finite element mesh of the designed multi-layer absorber with 447 eight-node brick elements and 1014 degrees of freedom. The flow resistivity of the porous material (glass fiber) $\sigma = 16000\,\mathrm{Ns/m^4}$, the plate thickness of the inner structure $t_i = 2\,\mathrm{mm}$ and the total thickness of this multi-layer absorber $t_t = 30\,\mathrm{mm}$. For experiments, four short cylinders with a diameter of 100 mm are arbitrarily cut from different positions of the designed multi-layer absorber and put into the impedance tube to measure their acoustic absorption coefficients respectively. As shown in Figure 12, each cylinder contains about four inner structure units shown in Figure 11. The averaged acoustic absorption coefficient of these cylinders is adopted to represent the acoustic absorption coefficient of the design multi-layer absorber. Figure 13 shows that the acoustic absorption of this designed multi-layer absorber is much better than that of the acoustic absorber without inner structure, except

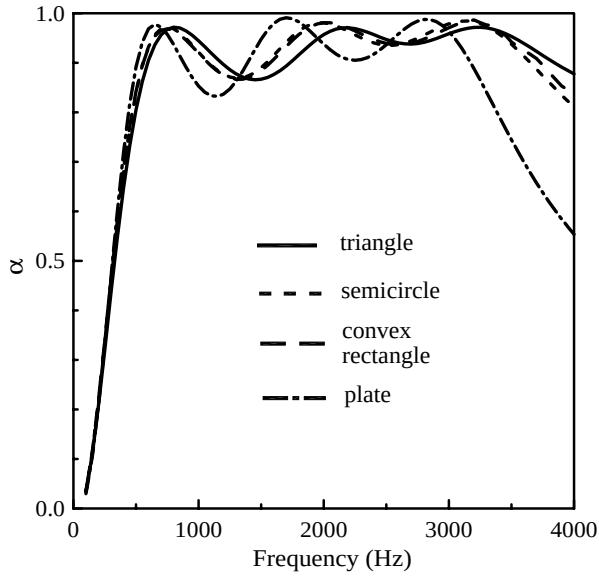

Figure 10. Comparison of the acoustic absorption coefficients for the multi-layer absorbers with various compartments.

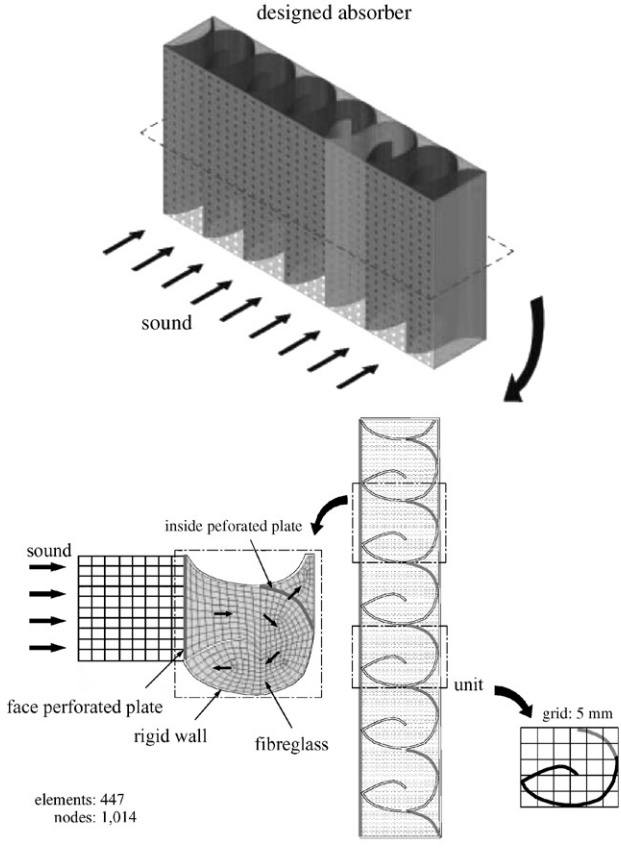

Figure 11. A novel design of the multi-layer absorber.

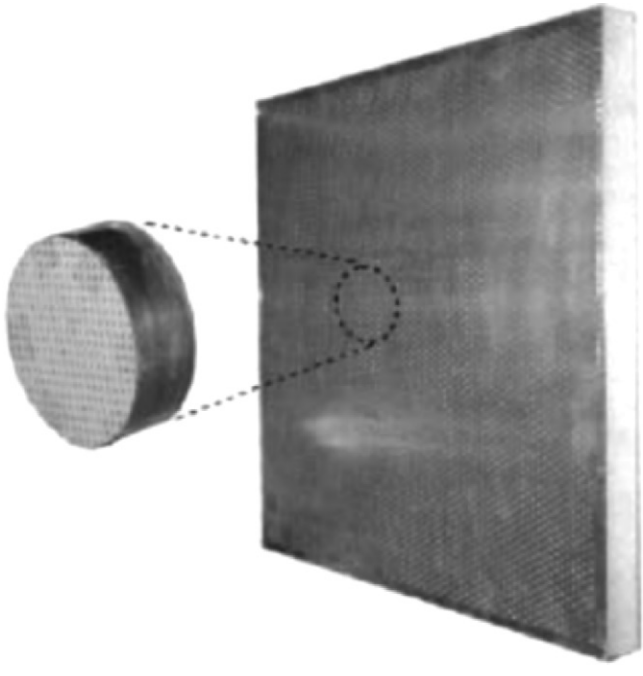

Figure 12. A short cylinder cut from the designed absorber.

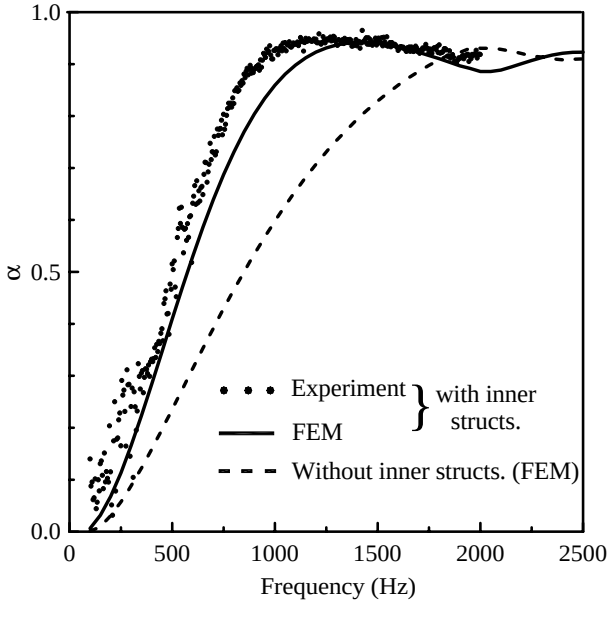

Figure 13. The acoustic absorption coefficients for the designed absorber.

at frequency bands over 1750 Hz. At frequency bands over 1750 Hz, the acoustic absorption of this designed multi-layer absorber does not have so significant effect as at lower frequency bands, but the acoustic absorption coefficient α of the designed multi-layer absorber still remains over 0·87. As expected, since the designed inner structure units

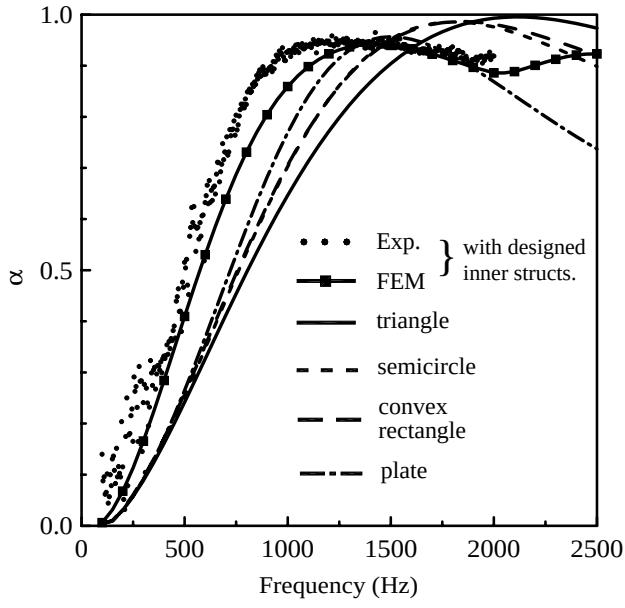

Figure 14. Comparison of the acoustic absorption coefficients for various multi-layer absorbers.

are assumed to be rigid in the finite element analysis, most of the experimental data obtained are higher than the finite element results.

The acoustic absorption of this designed multi-layer absorber is also compared with that of four types of basic inner structure compartments as mentioned in section 4.1. The geometric parameters of these basic inner structure compartments are the same as those in section 4.1 except that the porosity of the perforated plates and the total thickness are, respectively, changed to 8·7% and 30 mm. Figure 14 shows that this designed multi-layer absorber has good acoustic absorption especially at the frequency bands below 1250 Hz. However, as mentioned in section 4.1, the triangle, semicircle and convex rectangle shape compartments have better acoustic absorption characteristics at high frequencies.

5. CONCLUDING REMARKS

In this work, a rigorous finite element analysis model has been successfully applied to discuss the effect of different inner structures on the acoustic absorption of multi-layer absorbers. The results depict that more porous materials in front of the perforated plate will enhance the acoustic absorption at higher frequency bands, however, more porous materials behind the perforated plate will promote the acoustic absorption at lower frequency bands. Besides, the longer transmission path for the incident sound in acoustic absorbers will improve the acoustic absorption. Based on the above features, as an example, a newly designed multi-layer acoustic absorber with low thickness (30 mm) and high acoustic absorption is proposed. This would be helpful for the noise abatement in architecture or machine design.

REFERENCES

1. C. Zwikker and C. W. Kosten 1949 *Sound Absorbing Material.* New York: Elsevier.
2. M. E. Delany and E. N. Bazley 1970 *Applied Acoustics* **3**, 105–116. Acoustic properties of fibrous absorbent material.

3. A. Craggs 1978 *Journal of Sound and Vibration* **61**, 101–111. A finite element method for rigid porous absorbing materials.
4. D. A. Bies and C. H. Hansen 1980 *Applied Acoustics* **13**, 357–391. Flow resistance information for acoustical design.
5. V. Easwaran and M. L. Munjal 1993 *Journal of Sound and Vibration* **160**, 333–350. Finite element analysis of wedges used in anechoic chambers.
6. Y. J. Kang 1997 *Journal of the Acoustic Society of America* **102**, 3319–3332. Sound transmission through elastic porous wedges and foam layers having spatially graded properties.
7. W. H. Chen, F. C. Lee and D. M. Chiang 2000 *Journal of Sound and Vibration* **237**, 337–355. On the acoustic absorption of porous materials with different surface shapes and perforated plates.
8. D. F. Ross 1980 *Journal of Sound and Vibration* **69**, 509–518. A finite element analysis of parallel-coupled acoustic system using subsystems.
9. D. F. Ross 1981 *Journal of Sound and Vibration* **79**, 133–143. A finite element analysis of perforated compartment acoustic systems.
10. L. L. Beranek and I. L. Vér 1992 *Noise and Vibration Control Engineering*, 232–243. New York: John Wiley and Sons; Chapter 8.
11. A. Craggs 1979 *Journal of Sound and Vibration* **66**, 605–613. Coupling of finite element acoustic absorption models.
12. W. H. Chen and F. C. Lee 2001 *Journal of Sound and Vibration* **248**, 621–634. Acoustic transmission analysis of multi-layer absorbers.
13. W. A. Davern 1977 *Applied Acoustics* **10**, 85–112. Perforated facings backed with porous materials as sound absorbers - an experimental study.
14. M. L. Munjal 1987 *Acoustics of Ducts and Mufflers*, 254–284. New York: John Wiley and Sons; Chapter 7.